Dark Auroral Oval on Saturn Discovered in Hubble Space Telescope Ultraviolet Images

Lotfi Ben Jaffel,* Véronique Leers, Bill R. Sandel

Hubble Space Telescope ultraviolet images of Saturn obtained with the Faint Object Camera near 220 nanometers reveal a dark oval encircling the north magnetic pole of the planet. The opacity has an equivalent width of ~11° in latitude and is centered around ~79°N. The oval shape of the dark structure and its coincidence with the aurora detected by the Voyager Ultraviolet Spectrometer suggest that the aerosol formation is related to the auroral activity.

Aerosols and hazes are important components of Saturn's atmosphere. They play a prominent role in the atmosphere's heat budget, chemistry, and dynamics (*1*). Because these particles scatter and absorb sunlight, their vertical and horizontal distributions and, to a lesser extent, their nature can be retrieved from spectroscopic and imaging observations at different wavelengths. Ultraviolet (UV) wavelengths probe only the upper troposphere and the stratosphere (<100 mbar). The reflectivity of the planet at all latitudes is smaller than expected from a clear H_2 atmosphere (*1–3*), suggesting that dark materials are present in the upper atmosphere. The UV observations have revealed two distinct regions: (i) the low and mid-latitudes, at which tropospheric aerosols with sizes ~1 to 1.5 μm dominate and where the stratospheric particles, located at pressures ~30 to 70 mbar, are smaller (~0.1 μm) and less abundant, and (ii) the polar region (latitude >65°), which appears darker with aerosols located higher in the atmosphere (pressures <10 to 20 mbar).

Previous radiative transfer calculations (*2*) revealed that the polar absorbers differ in nature and abundance from those near low and mid-latitudes. A relation between the auroral ionization and aerosol formation has been long suspected because of the spatial correlation of both processes on Saturn (*4*). The aurora reported by the Voyager Ultraviolet Spectrometer (UVS) (*5*) lie poleward of 76° latitude, well within the dark polar region in the northern hemisphere. However, large uncertainties remained after the Voyager missions regarding the identity and energy of the precipitating charged particles and their ability to reach the homopause, where they can produce aerosols (*6*). Other processes have also been suggested for aerosol production, such as micrometeoroid bombardment and photochemistry (*7*), and the connection between aurora and polar haze has been uncertain.

We obtained two 895-s exposures of Saturn (Table 1) and part of its ring system over a 1.5-hour period on 26 June 1992 with the Faint Object Camera of the Hubble Space Telescope (HST/FOC) (Fig. 1A). The passband was centered near 220 nm with a full width at half maximum of 20 nm. This wavelength window is dominated by reflected sunlight. The count rate on the disc was near the saturation limit of the camera except in the dark polar region and in the rings. We therefore applied a linearity correction algorithm (*8*). In the images, the disc appears nearly uniform with a net limb darkening. The north polar region is conspicuously darker than other regions of the disc. A weak and unexpected enhancement of the reflectivity near the pole extends over almost ~1.5 arc sec. The corresponding region in the southern hemisphere is hidden by the 15.1° tilt. The derived reflectivity of the different components of the Saturn system are summarized in Table 2.

To quantify the structure near the pole, we took an east-west (E-W) cut 40 pixels wide (~1.5 arc sec) near the planet's center and a north-south (N-S) cut along the central meridian (Fig. 2A). To remove the steep gradient in reflectivity near the limb, we took the ratio of the N-S curve to the E-W distribution after scaling it to account for the flattening of the planet. Our radiative transfer calculation simulating the reflectivity in the N-S direction based on modeling of the planet's reflectivity from unaltered regions (*9*) gives consistent results. The ratio in Fig. 2A is almost 1 for $R/R_S < 0.78$ (R_S is the polar radius of Saturn) and decreases gradually toward the opaque region. However, after $R/R_S \sim 0.92$, the ratio increases to reach a plateau at ~0.97, which, surprisingly, corresponds to the pole. For $R/R_S > 0.98$, the ratio increases sharply before the two signals join. This enhancement cannot be a limb brightening because it is within the planetary disc (Fig. 2A). Processing of the second image led to the same findings. We conclude that the weak increase in reflectivity near Saturn's north pole is a real feature.

The center-to-limb distribution of reflectivity is modified by the camera point spread function. With the prominent characteristics of the planet's near-UV reflectivity unambiguously established, we deconvolved the images with the Lucy-Richardson technique (*10*). The restored images clearly reveal a symmetric, dark oval sur-

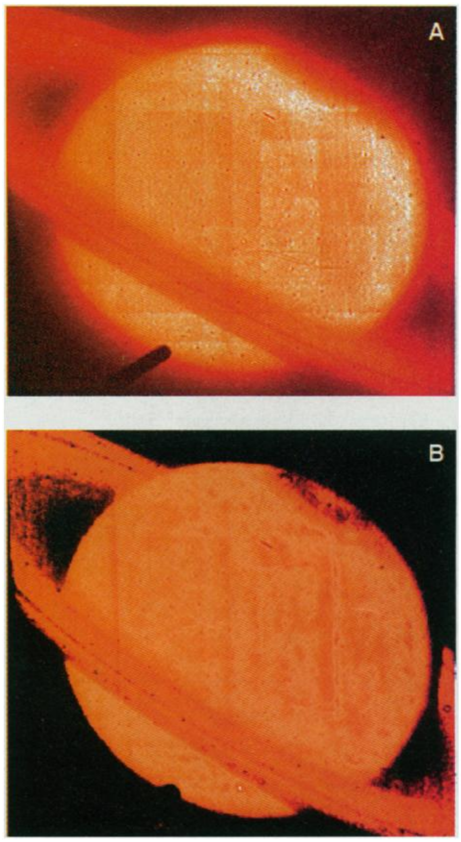

Fig. 1. (**A**) Saturn and its rings at 220 nm. The A and B rings and the Cassini division are visible against the dark sky and in front of the disc. The dark region near the top of the disc is the polar cap. (**B**) Image deconvolved with the Lucy-Richardson technique. The azimuthal symmetry of the dark oval is a result of the symmetry of the Saturn magnetic field. Any substantial tilt between the magnetic field and spin axis would break the symmetry because atmospheric diffusion would destroy the structure. This may be the case for Jupiter.

Table 1. Sequence of HST/FOC observations of Saturn on 26 June 1992. Abbreviations: UT, universal time; λ, wavelength; CML, central meridian longitude (System III); NUV, near ultraviolet.

Time (UT)	Central λ (nm)	CML (degrees)	Image
15:57	220	9	NUV1
17:25	220	58	NUV2

L. Ben Jaffel, Institut d'Astrophysique de Paris, Centre National de La Recherche Scientifique, F-75014 Paris, France.
V. Leers, Laboratoire de Physique Atmosphérique et Planétaire, Institut d'Astrophysique, Université de Liège, 4000 Liège, Belgium.
B. R. Sandel, Lunar and Planetary Laboratory, University of Arizona, Tucson, AZ 85721, USA.

*To whom correspondence should be addressed.

rounding the magnetic pole (Fig. 1B). The N-S and E-W (scaled to the N-S size of the planet) cuts across the restored image, as in Fig. 2A, lead to a reflectivity ratio similar to the one derived from the raw images (compare Fig. 2B with Fig. 2A). The absorption is stronger and the signal plateau is now followed by a slight drop. This drop is beyond the pole and is consistent with the far side of the oval. Such structure has been revealed by the HST observations in the UV aurora of Jupiter (*11*), but to our knowledge, this is the first observation of such an oval for Saturn. Surprisingly, it is observed in the near UV as an absorption, which is unique in our solar system.

The absorption in Fig. 1B has an equivalent width of 11° in latitude centered around ~79°N. The maximum absorption is near the edge of Saturn's polar cap, which lies in the range 75° to 78.7°N (*12*). The extinction maximum also falls near the latitude of the aurora detected by the Voyager UVS (*5*). The position of the southern aurora, a band between 78° and 81.5°S, was the better determined by Voyager. To compare it to our oval, we considered the N-S asymmetry of the magnetic field. If the magnetic fluxes through the polar caps are equal, the edge of the polar cap is about 1° nearer the pole in the north than in the south (*13*). Thus, the UVS observations in the south imply an aurora between 79° and 82.5°N, consistent with the HST images. The oval shape of the feature in Fig. 1B and its coincidence with the Voyager UVS aurora indicates that the polar haze is produced by energetic charged particles precipitating along the magnetic field lines from the magnetosphere into the atmosphere of Saturn.

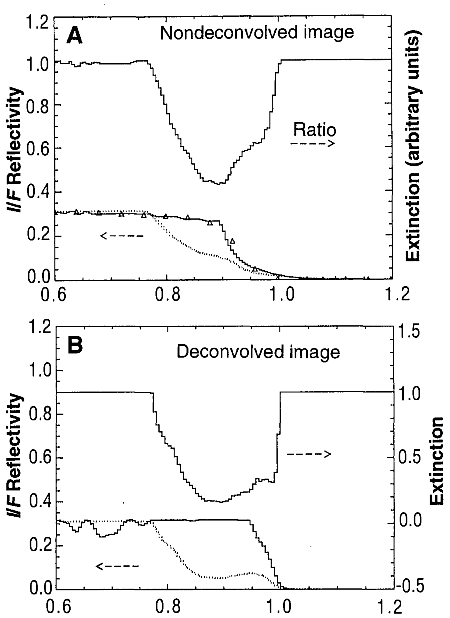

Fig. 2. (**A**) Scaled E-W (thick line near bottom) and N-S (dotted line) cuts across the image in Fig. 1A. This represents the disc reflectivity *I/F* versus the distance from the center in units of the Saturn polar radius R_S (*I* is the intensity of the reflected sunlight and πF is the incident solar irradiance). The E-W curve was scaled to the N-S size to account for the flattening of the planet. Note the weak bump in the N-S reflectivity beyond $0.92R_S$. The triangles show a N-S cut in the radiative-transfer model fit to the disc reflectivity. The ratio of the observed N-S to the scaled E-W curves is shown in the top curve. (**B**) Same as in (A) but for the deconvolved image shown in Fig. 1B. The feature beyond $0.92R_S$ is now more pronounced.

The polar aerosols are dark (*1, 2, 4*). This property is derived from several multispectral analyses, particularly with recent HST data, that clearly show the small value of the single-scattering albedo of these particles at wavelengths of 264 and 300 nm (*2, 3*). Also, occultation observations revealed that stratospheric aerosols are diffuse (*14*). Indeed, the opacity of the tropospheric aerosols seems to correlate well with atmospheric winds at all latitudes (*2, 15*). The distribution of the opacity from the pole location to lower latitudes (Fig. 2B) may thus represent the profile of the aurora-generated wind above the level of the haze production. At each latitude, the absorbers should be distributed above different heights.

For vigorous production of aerosols, the incident particles must deposit a part of their energy near or below the homopause (*6*). This implies that their energy is 5 to 10 keV or that the eddy diffusion coefficient K_H is stronger in the auroral region [compared to $K_H \sim 5 \times 10^6$ cm^2 s^{-1} at the equator (*16*)] so that the methane homopause is higher (*17*). The mass balance between production and loss of aerosols may constrain the efficiency of aerosol production (*4*), given an estimate of the energy flux of incoming particles. We estimate this energy flux at ~1.0 erg cm^{-2} s^{-1} using an auroral zone area of $\sim 1.8 \times 10^{18}$ cm^2 and an auroral power of 2×10^{11} W (*5*). The corresponding hydrocarbon ion production is $\sim 1.7 \times 10^{10}$ ions cm^{-2} s^{-1} for the $\sim 1.1 \times 10^{19}$ cm^2 equivalent area of the polar haze distribution inferred from Fig. 2B. We estimate that the aerosol loss rate for Saturn is $\sim 5 \times 10^{-14}$ g cm^{-2} s^{-1} (*18*). It follows that the efficiency factor should be ~0.9. This simple model confirms that aurora can produce the auroral haze.

Table 2. Averaged reflectivities at 220 nm. The individual reflectivity of each ring is provided. The global reflectivity of the rings system at 220 nm, as inferred by the International Ultraviolet Explorer (IUE) is also provided for comparison (*23*). All values are averages over the regions.

Regions	Reflectivity *I/F*
Disc	0.32
Equator	0.34
A ring	0.12
B ring	0.17
C ring	0.04
Rings (HST)	0.10
Rings (IUE)	0.09

REFERENCES AND NOTES

1. M. G. Tomasko, R. A. West, G. S. Orton, V. G. Tejfel, in *Saturn*, T. Gehrels and M. S. Matthews, Eds. (Univ. of Arizona Press, Tucson, 1984), pp. 150–194.
2. R. A. West *et al.*, *J. Geophys. Res.* **88**, 8679 (1983); E. Karkoschka and M. G. Tomasko, *Icarus* **106**, 428 (1993).
3. P. Winkelstein *et al.*, *Icarus* **54**, 309 (1983).
4. W. R. Pryor and C. W. Hord, *ibid.* **91**, 161 (1991).
5. B. R. Sandel and A. L. Broadfoot, *Nature* **292**, 679 (1981).
6. D. F. Strobel, in *The Photochemistry of Atmospheres*, J. S. Levine, Ed. (Academic Press, Orlando, FL, 1985), pp. 393–434.
7. V. G. Tejfel, *Int. Astron. Union Symp.* **65**, 415 (1974); R. G. Gladstone, thesis, California Institute of Technology (1983).
8. These observations were made before the corrective optics were installed. Up to 80% of the saturation value, the relation between the incident light flux and the count rate is well understood [C. R. Jenkins, *Mon. Not. R. Astron. Soc.* **226**, 341 (1987)]. We thus restricted our analysis to regions below 70% of the saturation level. This includes parts of the disc, the dark north polar cap (signal-to-noise ratio, ~32), and the rings.
9. The radiative-transfer adding-doubling method was used with the 40-stream approximation for Rayleigh scattering by H_2 and Henyey-Greenstein scattering by aerosol (*19*). The fit to the N-S direction is based on a two-layer model (*2*).
10. C. C. Cunningham and D. Anthony, *Icarus* **102**, 307 (1993).
11. V. Dols, J. C. Gérard, F. Paresce, R. Prangé, A. Vidal-Madjar, *Geophys. Res. Lett.* **19**, 1803 (1992); J. C. Gérard *et al.*, *Science* **266**, 1675 (1994).
12. N. F. Ness *et al.*, *Science* **212**, 211 (1981); K. W. Behannon, J. E. P. Connerney, N. F. Ness, *Nature* **292**, 753 (1981).
13. We extended equation 4 of (*20*) to include all terms in the Z_3 magnetic model (*21*). For each of a series of test latitudes near the aurora, we computed the magnetic flux though the circle at that latitude, then found the latitude in the other hemisphere characterized by the same value of the flux. Our estimate is consistent with the trend in the differences between N and S conjugate latitudes in table 1 of (*22*).
14. D. W. Smith, R. W. Shorhill, P. E. Johnson, E. Budding, A. S. Assad, *Icarus* **46**, 424 (1981).
15. R. A. West, A. J. Friedson, J. F. Appleby, *ibid.* **100**, 245 (1992).
16. G. R. Smith, D. E. Shemansky, J. B. Holberg, A. L. Broadfoot, B. R. Sandel, *J. Geophys. Res.* **88**, 8667 (1983).
17. R. G. Gladstone, *Eos* **70**, 1173 (1989).
18. R. A. West, D. F. Strobel, S. J. Kim, M. G. Tomasko, *Icarus* **65**, 161 (1986).
19. L. Ben Jaffel, C. Magnan, A. Vidal-Madjar, *Astron. Astrophys.* **220**, 306 (1988).
20. D. L. Chenette and L. Davis Jr., *J. Geophys. Res.* **87**, 5267 (1982).
21. M. H. Acuña, J. E. P. Connerney, N. F. Ness, *ibid.* **88**, 8771 (1983).
22. J. E. P. Connerney, *Geophys. Res. Lett.* **13**, 773 (1986).
23. L. W. Esposito *et al.*, in *Saturn*, T. Gehrels and M. S. Matthews, Eds. (Univ. of Arizona Press, Tucson, 1984), pp. 463–545.
24. L.B.J. acknowledges support from the Centre National de la Recherche Scientifique (CNRS) of France and from Institut National des Sciences de l'Univers (INSU) grant PNP-1994. V.L. is supported by the

Belgian National Fund for Scientific Research. The observations reported here are from the HST/FOC program (ID 1269; F. Paresce, principle investigator). This research is based on observations with the National Aeronautics and Space Administration (NASA)–European Space Agency (ESA) Hubble Space Telescope, obtained at the Space Telescope Science Institute, which is operated by the Association of Universities for Research in Astronomy under NASA contract NAS5-26555.

2 February 1995; accepted 28 June 1995

Urban Leakage of Liquefied Petroleum Gas and Its Impact on Mexico City Air Quality

Donald R. Blake and F. Sherwood Rowland

Alkane hydrocarbons (propane, isobutane, and *n*-butane) from liquefied petroleum gas (LPG) are present in major quantities throughout Mexico City air because of leakage of the unburned gas from numerous urban sources. These hydrocarbons, together with olefinic minor LPG components, furnish substantial amounts of hydroxyl radical reactivity, a major precursor to formation of the ozone component of urban smog. The combined processes of unburned leakage and incomplete combustion of LPG play a significant role in causing the excessive ozone characteristic of Mexico City. Reductions in ozone levels should be possible through changes in LPG composition and lowered rates of leakage.

Mexico City lies in a high valley surrounded by mountains capable of holding in pollutants released by its more than 15 million inhabitants and has suffered during the past two decades from increasingly severe smog events with very high ozone (O_3) levels (*1*, *2*). The Mexican 1-hour criterion for O_3 is 0.11 parts per million (ppm; US Environmental Protection Agency, 0.12 ppm; World Health Organization, 0.10 ppm) and was exceeded in Mexico City on 71% of the days in 1986 and 98% in 1992, with values as high as 0.48 ppm on 16 March 1992 (*3*). Previous investigations of O_3 formation in Mexico City have primarily emphasized the release of hydrocarbons (HCs) from automobiles and trucks, and secondarily in industrial plants (*4*). Current control mechanisms during periods of high O_3 call for reductions in the use of automobiles and in levels of industrial operation. However, our detailed chemical analysis of the specific HC composition of Mexico City air (*5*, *6*) has consistently shown very high concentrations of the C_3 and C_4 alkanes not usually found as more than very minor components in vehicular or industrial emissions. In most of our air samples, these three alkanes were the dominant nonmethane HCs (NMHC), with concentrations exceeding those of well-known signature compounds for fossil fuel combustion, such as ethylene and acetylene. The source of these alkanes lies in LPG—the major energy source for cooking and heating in urban households in Mexico City—leaking in unburned form into the atmosphere on a massive scale. These reactive HCs, together with the olefinic minor components in LPG, plus olefinic and acetylenic products from their incomplete combustion, play a major (perhaps the dominant) role in O_3 production in the Valley of Mexico.

Department of Chemistry, University of California, Irvine, CA 92717, USA.

Previous studies have recognized the very high NMHC concentration in Mexico City air (*7*), and that standard emission inventories have fallen short by a factor of 4 in quantitative explanation of their presence (*8*). No controls on LPG emissions are currently specified in Mexico City, nor have any been specifically proposed (*9*). Substantial progress toward reduction of urban O_3 formation seems possible if attention is directed toward the problems associated with LPG usage. Although control of O_3 formation by reduction in HC emissions is less effective in areas such as Mexico City with a high ratio of NMHC to nitrogen oxides (NO_x), the overall HC reactivity of LPG is very dependent on its particular composition, especially in olefinic content as discussed below.

The formation of additional O_3 in the troposphere involves a combination of sunlight with excess concentrations of HCs and NO_x as in reactions 1 to 5 (*10*, *11*) (*R* is an alkyl group; $h\nu$ is a photon; M is a third-body molecule):

$$HO + RH \rightarrow H_2O + R \qquad (1)$$

$$R + O_2 \rightarrow RO_2 \qquad (2)$$

$$RO_2 + NO \rightarrow RO + NO_2 \qquad (3)$$

$$NO_2 + h\nu \rightarrow NO + O \qquad (4)$$

$$O + O_2 + M \rightarrow O_3 + M \qquad (5)$$

Subsequent reactions of the various RO species such as aldehydes and ketones from reaction 3 are also important. A useful approximation to the relative importance of individual HCs in urban O_3 production can be obtained from the measured HC composition multiplied by the known rate constants for reaction with OH radical in reaction 1 (*12*). These evaluations require quantitative measurements of ambient HC concentrations, and careful laboratory eval- uation of the corresponding rate constants for reaction with each (*13*). A better approximation for O_3 formation in the urban environment can probably be obtained through the maximum incremental reactivity (MIR) estimates of Carter (*14*), who takes into account the subsequent reactions which follow the initial OH attack on the HCs.

The concentrations for selected HC compounds found in four representative air samples collected in February 1993 (*5*, *6*) are given in Table 1 in parts per billion by volume (ppbv). Zocalo is in the central part of Mexico City, and canisters were filled there at 6 a.m. and noon during four consecutive days in the Plaza de la Constitucion. The Pyramid of the Moon, on the other hand, is ~50 km northeast of the city center and was in an upwind direction from the city on 21 February. The measured HC concentrations there are generally comparable to those expected in locations well separated from local sources, except for those of propane and the two butanes, which are substantially above usual remote levels. Away from urban sources, the concentration of ethane normally exceeds those of propane and each of the butanes, in part because the atmospheric lifetime of ethane is considerably longer. In contrast, the Tlalpan Highway sample was taken in the midst of heavy afternoon traffic, and contains a substantial admixture of gases from vehicular emissions (such as ethylene, acetylene, and isopentane). The decrease in concentration of propane and the butanes between 6 a.m. and noon is a regular occurrence associated with the daylight expansion of the planetary boundary layer from the early morning 100 to 300 m above ground level to late afternoon elevations of about 2000 m above ground level (*15*).

Very high concentrations of propane, *n*-butane, and isobutane dominate the NMHC molar fractions except in heavy traffic conditions. The molar ratios among these three alkanes are quite similar in the two Zocalo air samples of Table 1, as they were in the other six collected at the same location. These HC ratios and their standard deviations are shown in Table 2 for the eight Zocalo samples and for seven canisters each collected in three other locations around the city. The remaining canisters were filled at various times of day in about 45 locations scattered all over the metropolitan area. For comparison purposes, we note that the reported concentration of propane was 1.6 ppbv for noontime summer measurements in Atlanta (*16*), and that the median concen-